Toward Economical Purification of Styrene Monomers: Eggshell Mo_2C for Front-End Hydrogenation of Phenylacetylene

Min Pang, Zhengfeng Shao, Xinkui Wang, and Changhai Liang
Laboratory of Advanced Materials and Catalytic Engineering, Dalian University of Technology, Dalian 116024, P.R. China

Wei Xia
Laboratory of Industrial Chemistry, Ruhr University of Bochum, Bochum 44780, Germany

DOI 10.1002/aic.14822
Published online April 22, 2015 in Wiley Online Library (wileyonlinelibrary.com)

An eggshell Mo_2C catalyst which is designed from the rapid combination of molybdate with melamine is described. In contrast to Pd-based catalysts, the eggshell Mo_2C operates effectively with a wide-concentration window in high-temperature gas phase hydrogenation of phenylacetylene, thus, an economical and energy-efficient front-end purification of styrene monomers might be possible. © 2015 American Institute of Chemical Engineers *AIChE J*, 61: 2522–2531, 2015
Keywords: carbide, eggshell, front-end, phenylacetylene, hydrogenation

Introduction

The partial hydrogenation of phenylacetylene (PA) has been an important industrial process for the synthesis of high-purity styrene (ST), which is used as the monomer for the synthesis of polystyrene, a widely used class of thermoplastic. Commercial ST derived from the dehydrogenation of ethylbenzene (EB) typically contains a small fraction of PA of up to 150 ppm. Despite its low concentration, PA has detrimental effects on the polymerization rate, and could induce undesired cross-linking of polymer chains.[1] To meet this stringent standard for monomer purity, the level of PA should be reduced to $<$10 ppm. For this purpose, a catalytic partial hydrogenation process has been developed to reduce the amount of PA into the lower ppm range with minimal influence on the dominating ST. Supported palladium catalysts, for example, on carbon nanotubes, Si-Al-O, zeolites, TiO_2, polymers, and more recently C_3N_4 are used for the hydrogenation reactions.[2–7] Pd selectively hydrogenates traces of alkynes to alkenes under alkene-rich conditions.[8] However, in addition to the high cost, Pd suffers from rapid activity loss on contact with infinitesimal amounts of impurities in the feedstock, which hinders its long-term industrial applications. Therefore, modification of Pd by a second metal was examined to extend the service life of the catalysts. The incorporation of heteroatoms, such as Ag, Ga, or Cu, is able to alter the electronic structure of Pd by forming alloys, thus, allowing a quick desorption of the carbonaceous species from the catalyst surface.[9–11] Consequently, the formation of carbon overlayers and, in particular, the oligomerization of the reactive intermediates to higher hydrocarbons which caused catalyst fouling can be decreased by several orders of magnitude. Many ways have been proposed to control the performance of Pd in alkene hydrogenation, including modifying the electronic properties by alloying with other metals, exposing the specific type of active sites or lattice plane,[12,13] changing the interplay with the surroundings,[14,15] uncrystallizing through the introduction of nonmetals,[16] and so forth. One typical case was the use of surfactants inherited from the synthetic process to improve the alkene selectivity by modifying the electronic environment of Pd through N-containing species.[17,18] However, the surfactant-wrapped Pd particles normally cannot be effectively stabilized by the supports, thus causing a leaching problem. Controlling the morphology of Pd to exclusively expose the appropriate lattice planes for partial hydrogenation of alkyne was another way to enhance the alkene selectivity. However, to immobilize these Pd particles without losing the exposure of the required lattice planes remains a big challenge. Other option such as the less active Au-based catalysts were frequently investigated for alkyne hydrogenation, but the alkyne conversions in these cases were not satisfactory.[19,20] Recently, increasing demands for more economical processes for alkyne hydrogenation have triggered a fast-developing research area of new catalytic materials based on nonprecious metals. A series of multicomponent catalysts based on Ni and Cu using Fe, Al or Zn as modifiers displayed a good level of alkene selectivity of up to 80%, indicating noble metal-free catalytic system has started to play an important role in this area of reseach.[21–24]

The existing process of PA hydrogenation is performed in liquid phase below 100°C. Elevating temperature obviously induces overhydrogenation with using those aforementioned catalysts. In industry, conducting a process at low temperature is, however, against the block integration and should be avoided for high energy efficiency. In addition, increasing the operating temperature to perform the hydrogenation in

Correspondence concerning this article should be addressed to C. Liang at changhai@dlut.edu.cn.

Table 1. Summary of Catalyst Preparation

Type of Catalyst	Powder Mo_2C	Eggshell Mo_2C/γ-Al_2O_3	Powder Mo_2C/γ-Al_2O_3	Eggshell MoO_x/γ-Al_2O_3
Physical state	Powder	Spherical extrudate	Powder	Spherical extrudate
Reagents	AHM,MA	AHM,MA	AHM,MA	AHM
Wet chemistry	Mixing	Impregnation	Impregnation	Impregnation
Post treatment	Thermal decomposition	Thermal decomposition	Thermal decomposition	Hydrothermal reduction

gas phase could enhance catalyst stability. As desorption of carbonaceous species from the catalyst surface is accelerated in gas phase, the deactivation due to extensive oligmer production could be reduced to a larger extent should the reaction temperature be properly selected. Therefore, noble metal-free is just one of the criteria for competitive advantage. Good performance in terms of suppressing overhydrogenation and oligmerization in gas phase PA hydrogenation shall be the main focus in future development of alternatives to the commercial Pd-based catalysts.

Earlier work revealed the formation of carbide-like phase of Pd during the early stage of Pd-catalyzed alkyne hydrogenation. The formation of carbides on the surface region was proposed to be responsible for the constantly high selectivity to alkenes.[25] While the actual role of the carbides in alkyne hydrogenation is still under debate, this part of work did inspire us to compile the carbides into the catalog of potentially advantageous catalytic materials. Early transition metal carbides showed some reagent adsorption and activation phenomena that were qualitatively similar to those observed on precious group metals, though reaction rates were several orders of magnitude slower. This property of transition metal carbides may help promoting the selectivity of the intermediates in certain consecutive reactions usually catalyzed by noble metals due to the slow activating of the intermediates with respect to the relatively quick desorption of the intermediates over the carbides. In this work, we conducted the PA hydrogenation under industrially relevant conditions over a series of molybdenum carbide catalysts. The results indicated that the carbide phase was intrinsically less capable in activating ST thus able to terminate the hydrogenation at the intermediate step. In addition, molybdenum carbides showed both high activity and selectivity during PA hydrogenation with high H_2/PA ratios close to those in the tail-end cuts of an EB dehydrogenation process. The hydrogenation process thus can be possibly coupled with EB dehydrogenation to develop a more economical front-end technology for the purification of ST.

Experimental

All the reagents were purchased from Sinopharm Chemical Reagent Co., and used without further purification. The γ-Al_2O_3 pellets with a mean diameter of 5 mm, a surface area of 280 m^2/g, a total pore volume of 0.46 cc/g, and an average mass of 70 mg were used as received without removal of the residual polymers which were used as binding agents. Table 1 depicts the summary of the catalyst preparation, while the preparation details are presented below.

Powder Mo_2C

The powder Mo_2C was prepared by a single step of pyrolysis of the Mo^{VI}-melamine hybrids (chemical formula: $Mo_{19}O_{66}(C_3H_7N_6)_{18}\cdot 12H_2O$) under a flow of H_2/Ar (v:v = 2:5, 70 mL/min) at 650°C for 90 min. Mo^{VI}-melamine hybrids were obtained by mixing the aqueous solutions of ammonium molybdate ($(NH_4)_6Mo_7O_{24}\cdot 4H_2O$) and melamine ($C_3H_6N_6$) and collecting the immediately precipitated white solids. The as-prepared powder Mo_2C possessed a surface area of 7 m^2/g.[26]

Eggshell Mo_2C/γ-Al_2O_3

In the preparation of eggshell Mo_2C/γ-Al_2O_3, γ-Al_2O_3 pellets were impregnated in $(NH_4)_6Mo_7O_{24}$ (aq.) in an appropriate quantity for obtaining a Mo loading of 10 wt %. After 24 h of impregnation, the γ-Al_2O_3 pellets were collected from $(NH_4)_6Mo_7O_{24}$ (aq.) without drying and added into melamine (aq.). The γ-Al_2O_3 pellets were collected by filtration after conditioned to melamine (aq.) for 10 min and dried at 120°C before further heat treatment under a flow of H_2/Ar (v:v = 2:5, 70 mL/min) at 650°C for 90 min.

Powder Mo_2C/γ-Al_2O_3

Powder γ-Al_2O_3 (by grinding the γ-Al_2O_3 pellets into fine powder) were impregnated in $(NH_4)_6Mo_7O_{24}$ (aq.) in an appropriate quantity for obtaining a Mo loading of 10 wt %. Melamine (aq.) was added into the slurry containing powder γ-Al_2O_3 after 24 h of impregnation. The powder γ-Al_2O_3 was collected by filtration after conditioned to melamine (aq.) for 10 min and dried at 120°C before further heat treatment under a flow of H_2/Ar (v:v = 2:5, 70 mL/min) at 650°C for 90 min.

Eggshell MoO_x/γ-Al_2O_3

The eggshell MoO_x/γ-Al_2O_3 was used as a reference. Its preparation was identical to that of the eggshell Mo_2C/γ-Al_2O_3 without subjecting the impregnated γ-Al_2O_3 pellets to melamine (aq.).

PA hydrogenation

The gas-phase PA hydrogenation (Reaction scheme seen in Fig. 1) was performed in a fixed-bed continuous-flow cylindrical stainless steel reactor which was 12 mm in diameter of the cross-section, 2 mm in wall thickness, and 500 mm in length. For each reaction, a certain amount of catalyst, that is, a pellet of eggshell Mo_2C/γ-Al_2O_3 or eggshell MoO_x/γ-Al_2O_3, 0.07 g of powder Mo_2C/γ-Al_2O_3, and 0.007 g powder Mo_2C were used in each case for obtaining identical amount of Mo. They were then diluted with 2 g of quartz sand and placed in the thermostatic region of the reactor, which was about 30 mm in length at the middle of the reactor. All the catalysts were reduced *in situ* at 0.5 MPa H_2 (50 mL/min) at 400°C for 120 min prior to the hydrogenation. The feedstock consisted of a solution of 1 wt % PA in cyclohexane (unless otherwise mentioned) and was fed into the reactor by a high performance liquid chromatography (HPLC) pump. The feed rates of the reactants were expressed at liquid state. Liquid samples were collected from a trap cooled in cold water at the bottom of the reactor. The samples were analyzed using Agilent 7890-II gas

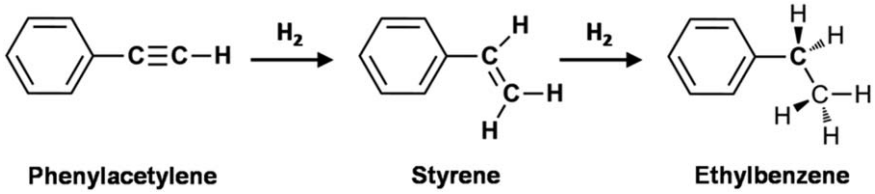

Figure 1. Reaction scheme of the consecutive PA hydrogenation to ST and EB.

chromatography equipped with an OV-101 capillary column and a flame ionization detector, and confirmed by gas chromatography-mass spectrometry. Liquid samples were collected after a stabilizing period of 12 h for evaluating the performance of the catalysts. The weight hourly space velocity (WHSV) and the styrene loss (ST_{Loss}) were calculated using the following equations:

$$\mathrm{WHSV} = \mathrm{Mass\ Flow}_{[PA]}/\mathrm{weight\ of\ cat}$$
$$= [\mathrm{Feed\ Rate/mL/min}] \times 60 \times 0.78 \times 0.01/0.007$$
$$\mathrm{ST_{Loss}} = \left\{[ST]_{initial} - [ST]_{final}\right\}/[ST]_{initial}$$

Characterization

X-ray diffraction (XRD) patterns were recorded on a Rigaku D/MAX2400 diffractometer with Cu Kα (40 kV, 100 mA) radiation. All samples were ground into fine powder before testing. Transmission electron microscopy (TEM) was performed on a Philips CM200 FEG transmission electron microscope with an accelerating voltage of 200 kV. X-ray photoelectron spectroscopy (XPS) measurements were performed in an ultrahigh vacuum setup equipped with a Gammadata-Scienta SES 2002 analyzer and used the main C 1s peak at 284.5 eV as reference. The line distribution profile of Mo, C elements in the cross-section of γ-Al_2O_3 pellets was measured using electron probe microanalyzer in EPMA-1600. Carbon, hydrogen, and nitrogen (CHN), elemental analysis was performed with an Elementar Vario EL system. The hemisphere of γ-Al_2O_3 was embedded in a thermoplastic resin with the polished cross-section upward and coated with a layer of gold by vacuum deposition. The acceleration voltage of the electron beam was 15 kV and the sample current was 0.012 μA. The electronic signals were collected with a scanning speed of 0.001 mm/s. CO chemisorption was measured using ASiQC0000-4 (Quantachrome Instrument Co.). Samples were treated in H_2 flow at 673 K for 2 h and evacuated at 5×10^{-2} Pa for 2 h before chemisorption measurements at 303 K. The Mo content of powder Mo_2C was determined with a Cahn TG-2131 thermobalance in pure air with a heating rate of 5°C/min from room temperature to 800°C. Temperature-programmed oxidation (TPO) was performed by introducing 5% O_2/He with a total flow rate of 100 mL/min into the system while the temperature was raised from RT to 900°C at a rate of 10°C/min. The signal of H_2O (m/e = 18), CO (m/e = 28), and CO_2 (m/e = 44) were monitored.

Results and Discussion

Formation process of eggshell Mo_2C/γ-Al_2O_3

Previous work by our group has shown a cheap single-source precursor for β-Mo_2C obtained by combining ammonium molybdate (aq.) with melamine (aq.).[26] The mixing immediately produced resin-like white solids, which possessed a large molecular weight of 5382. Through a single step of heat treatment at 650°C, the white solids were transformed into highly pure β-Mo_2C with almost exactly the same as the stoichiometric amount of carbon (Eq. 1)

$$\mathrm{Mo_{19}O_{66}(C_3H_7N_6)_{18}\cdot 12H_2O} \rightarrow \frac{19}{2}\mathrm{Mo_2C} + \mathrm{xCO} + \mathrm{yCO_2} + \frac{76+\mathrm{x}}{3}\mathrm{N_2} + \frac{4\mathrm{x}+6\mathrm{y}-95}{3}\mathrm{NH_3} + (78-\mathrm{x}-2\mathrm{y})\,\mathrm{H_2O} + \frac{89-2\mathrm{x}-2\mathrm{y}}{6}\mathrm{C_3H_6N_6} \quad (1)$$

In this work, we have used this synthetic route to prepare three types of Mo_2C catalysts: powder Mo_2C, powder Mo_2C/γ-Al_2O_3, and eggshell Mo_2C/γ-Al_2O_3 for assessment. After impregnation with aqueous solution of ammonium molybdate, Mo species showed an eggshell distribution on the γ-Al_2O_3 extrudate (Figure 2a). Gibson et al. explained this phenomenon well using *in situ* noninvasive spectroscopic techniques and reconstructed the evolution of $Mo_7O_{24}^{6-}$ within the γ-Al_2O_3 extrudate during the impregnation.[27] Mo species were inhibited from entering the centre of the γ-Al_2O_3 extrudate due to the strong electrostatic interaction between $Mo_7O_{24}^{6-}$ and Al-OH^{2+}, which gave rise to an Anderson-type heteropolyanion of $Al(OH)_6Mo_6O_{18}^{3-}$ (Eq. 2). A gradient of Mo components toward the core of the extrudate formed as a consequence

$$12\mathrm{Mo_7O_{24}^{6-}} + 7\mathrm{Al_2O_3} + 27\mathrm{H_2O} + 30\mathrm{H^+} \rightarrow 14\mathrm{Al(OH)_6Mo_6O_{18}^{3-}} \quad (2)$$

When subjecting the impregnated γ-Al_2O_3 extrudate to melamine (aq.), the protonated —NH_2 moieties of the melamine molecules reacted with the adsorbed $Mo_7O_{24}^{6-}$ species in a very fast way leading to the formation of Mo^{VI}-melamine hybrids (single-source precursors for β-Mo_2C) *in situ* bounded by Al-OH^{2+}. Due to a large molecular weight of about 5400 and a huge steric hindrance, the hybrids could effectively block the pores of the supports thus, prohibiting the inward diffusion of the melamine molecules. Through a single step of heat treatment at 650°C, the hybrids converted into islands of β-Mo_2C dispersed on the outer layer of the γ-Al_2O_3 extrudate with identical inward depth, thus were described as a carbide shell.

Characterization of eggshell Mo_2C/γ-Al_2O_3

Elemental distribution vs. diameter was measured by electron probe microanalysis (EPMA) operating in line scanning mode. No carbon signal was captured across the γ-Al_2O_3 body (Figure 2b). We presumed the thickness of the carbide layer was less than the measuring step of EPMA of 1 μm, or otherwise was nanometer sized. The C content in the

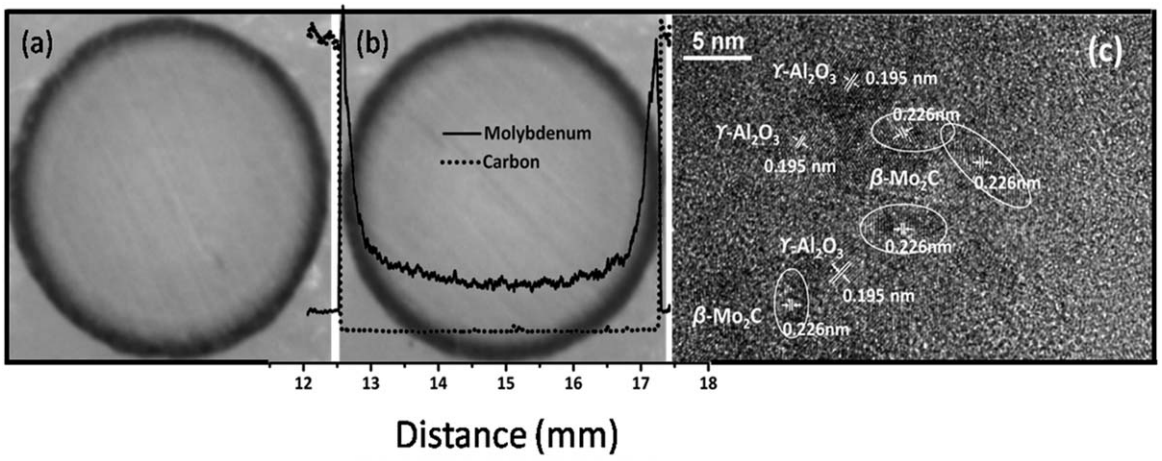

Figure 2. Optical images of the cross-sections of the eggshell MoO_x/γ-Al_2O_3 (a) and eggshell Mo_2C/γ-Al_2O_3 (b). Attached is the elemental distribution of Mo (solid) and C (dots) along the diameter. The plateau of carbon beyond but close to the γ-Al_2O_3 pellet was due to the thermoplastic polymers used as fixed agents during the measurements. (c) High-resolution TEM image of the sample scratched off the surface of the eggshell Mo_2C/γ-Al_2O_3. The measured distance of 0.195 nm was attributed to some crystallized γ-Al_2O_3 after the heat treatment.

eggshell Mo_2C/γ-Al_2O_3 was estimated as 0.05 wt % after eliminating the contribution from the γ-Al_2O_3 extrudate (Table 2). By referring to the C content, the thickness of the carbide layer could be roughly estimated based on three assumptions: (1) all of the carbon arose from the carbide phase; (2) no other carbide phases (e.g., MoC, MoC_{1-x}) except Mo_2C existed in the catalyst; (3) the carbide layer was described as a spherical shell filled with Mo_2C particles but without condensation. In this way, the carbide layer was calculated to be 800 nm in thickness. While given that part of the carbon was amorphous (e.g., surface carbon deposit) and the existence of other carbide phases with higher C content, the actual carbide layer should be much thinner. To confirm the presence of the carbide phase in the eggshell Mo_2C/γ-Al_2O_3, the sample was studied by TPO. The powder Mo_2C (verified by XRD patterns from Figure 3a) prepared by the thermal treatment of the Mo^{VI}-melamine hybrids was used as a standard carbide for comparison during heating in oxidizing atmosphere (i.e., O_2-He mixture). As shown in Figure 4, the oxidation of the eggshell Mo_2C/γ-Al_2O_3 occurred in two distinct regimes, almost identical to the case of the powder Mo_2C. The first regime in the profile from 280 to 450°C belonged to the surface oxidation of molybdenum carbide, while the second regime from 450 to 700°C was derived from the bulk oxidation of molybdenum carbide, the rate of which was determined by the diffusion of oxygen atoms within the particles. Thus, the second regime in the case of the eggshell Mo_2C/γ-Al_2O_3 was observed to end at lower temperature with respect to the powder Mo_2C for the fast diffusion of oxygen atoms within the small dispersed carbide particles supported on the Al_2O_3 support. The deconvoluted Mo 3d XPS spectrum of the eggshell Mo_2C/γ-Al_2O_3 gave rise to Mo species with binding energy of 228.2 eV (Figure 5a), which can be assigned to carbidic Mo.[28,29] Further evidence on the carbide phase was from the high-resolution TEM image, in which the measured lattice distance of 0.226 nm was indexed to the (101) facet of β-Mo_2C (Figure 2c). Based on the results, the hierarchical structure of the eggshell Mo_2C/γ-Al_2O_3 can be described in analogy to an egg with MoO_x as the eggshell wrapped by a nanolayer of Mo_2C.

Molybdenum carbide catalysts in PA hydrogenation

Table 3 depicts the hydrogenation performance of the catalysts as a function of WHSV. It can be seen from the initial results that decreasing WHSV over powder Mo_2C did not cause any obvious decrease in the selectivity to ST while the

Table 2. Mo, Mo_2C, C Contents, CO Uptake, and TOF

	Content (wt %)				
Sample	Mo[a]	C[b]	Mo_2C[c]	CO Uptake (μmol/g)	TOF[d] (min^{-1})
γ-Al_2O_3	–	0.37	–	–	–
Eggshell Mo_2C/γ-Al_2O_3	0.63	0.05[e]	0.85	–[f]	7.2[g]
Powder Mo_2C/γ-Al_2O_3	1.54	0.11[e]	1.87	–[f]	3.4[g]
Powder Mo_2C	93.3[h]	4.5[i]	–	25.9	1.1×10^{4}[j]

[a]By ICP-AES.
[b]Averaging the results of three times of analysis.
[c]Calculated by assuming carbon arose from Mo_2C and no other carbide phases existed.
[d]Of the reaction state depicted in Table 3, Entry 8.
[e]Eliminating the contribution from alumina extrudate.
[f]Cannot measure with acceptable accuracy due to the actual Mo_2C loading was ultralow.
[g]On the basis of the total Mo_2C loading.
[h]By thermogravimetric (TG) analysis.
[i]By CHN elementary analysis.
[j]On the basis of the CO uptake assuming 1:1 stoichiometry for CO and Mo_2C. TOF was calculated according to the formula: $TOF = (F \times X)/M$; where F is the molar rate of the reactant, X is the PA conversion, and M is the mole of Mo_2C.

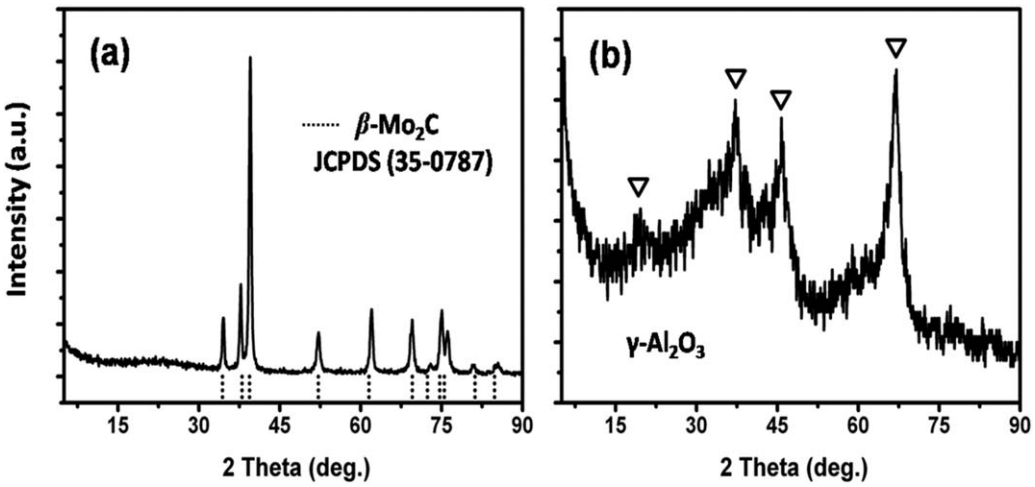

Figure 3. XRD patterns of (a) powder Mo_2C and (b) eggshell Mo_2C/γ-Al_2O_3.

No diffraction peaks due to Mo species except the background for γ-Al_2O_3 were resolved in (b) owing to a low loading and corresponding high dispersion of Mo species, while all resolved peaks in (a) can be well indexed to β-Mo_2C with a hexagonal structure.

PA conversion showed a gradual increase. This phenomenon indicates that β-Mo_2C was intrinsically less effective in activating ST. To the best of our knowledge, molybdenum carbides have not been applied for PA hydrogenation in the literature so far. The observed high selectivity cannot be fully understood at this stage. It can be correlated with the incorporation of carbon to Mo forming carbide, which was demonstrated to have properties similar to noble metals in the context of catalytic activity and selectivity.[30–32]

The macroscopic eggshell distribution which localizes the active phase on the periphery of the support can minimize the inner diffusion of the reactants, thus improving the mass transfer for a high-catalytic efficiency. Furthermore, the readsorption of the reaction intermediates over the catalysts in eggshell distribution can be significantly reduced, which is beneficial for a high selectivity to the intermediate products in consecutive reactions.[33,34] Thus, we expected the use of the eggshell Mo_2C/γ-Al_2O_3 could maintain the high selectivity to ST at high PA conversion. Remarkably, the eggshell Mo_2C/γ-Al_2O_3 was found to facilitate a high selectivity toward ST, in line with a significantly enhanced PA conversion compared with the powder Mo_2C under identical WHSV.

Powder Mo_2C/γ-Al_2O_3 was comprised of aggregates of microeggshell primary particles, giving rise to a porous network in the interstitial spaces between them. It seems that readsorption of the intermediates within this porous network of primary particles produced the observed lower selectivity to ST compared with that over the eggshell Mo_2C/γ-Al_2O_3 under identical conditions.

Molybdenum oxides in PA hydrogenation

Molybdenum oxides were observed in both the eggshell and the powder Mo_2C/γ-Al_2O_3 (Mo 3d XPS spectrum shown in Figure 5b). In an attempt to understand their roles in the reaction, we compared the catalytic performance of the eggshell Mo_2C/γ-Al_2O_3 directly with that of the counterpart, the eggshell MoO_x/γ-Al_2O_3, during a long-term PA hydrogenation (Figure 6). The results implied that the eggshell MoO_x/γ-Al_2O_3 was undergoing a progressive change in the surface region, as indicated by the gradual increase in both the PA conversion and the selectivity to ST. After a time period of

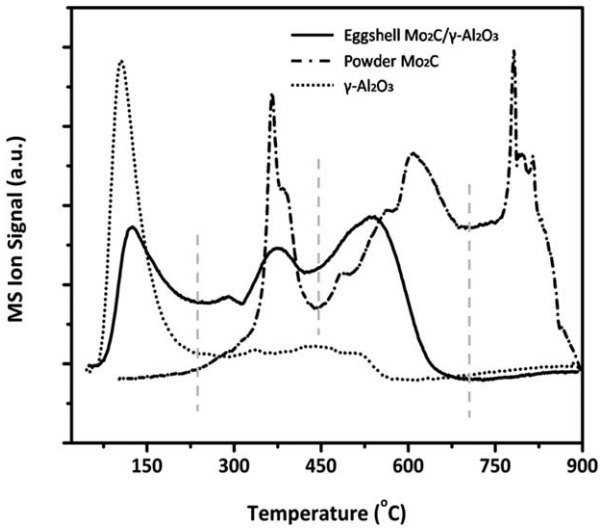

Figure 4. CO_2 profiles in the TPO of the γ-Al_2O_3, eggshell Mo_2C/γ-Al_2O_3, and powder Mo_2C.

The oxidation of the powder Mo_2C occurred in three distinct regimes. The first regime ranging from 280 to 450°C belongs to the surface oxidation of Mo_2C, whereas the second regime from 450 to 700°C is assigned to the bulk oxidation of Mo_2C. Normally, the CO_2 signals disappear from here onward owing to the complete oxidation of Mo_2C. However in the present case, a sharp increase of CO_2 signals appeared at around 780°C. The oxidation of Mo_2C is determined by the inward diffusion of oxygen. When the particle size of Mo_2C is big or the particles agglomerate severely, it is possible for a core (Mo_2C)-shell (MoO_3) structure in the oxidation progress. The MoO_3 shell will slow down the diffusion of oxygen into the bulk and shields the Mo_2C core from being oxidized. While the temperature increases continuously, the sublimation of MoO_3 becomes distinct. The Mo_2C core loses protection owing to the elimination of MoO_3 shell and will be oxidized rapidly due to the accelerated oxygen diffusion at elevated temperature. The powder Mo_2C was characterized by micrometer-sized agglomerate in our previous work, so it is reasonable to observe an additional oxidation region in the range of 750–840°C. Referring to the γ-Al_2O_3, CO_2 released in the range of RT-280°C in the case of eggshell Mo_2C/γ-Al_2O_3 is attributed to those physisorbed on the γ-Al_2O_3 extrudate.

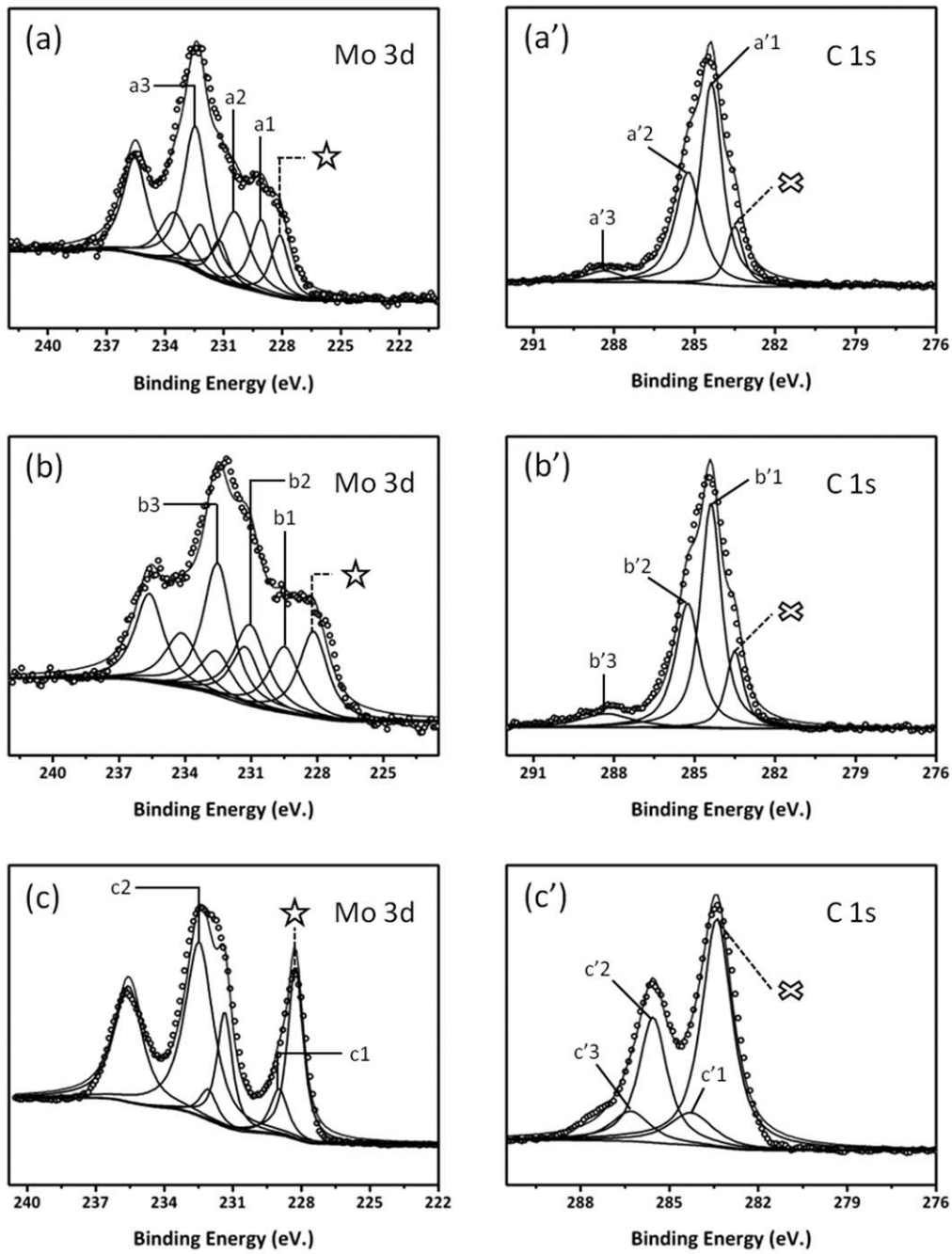

Peak Assignment (unit: eV)								
image	Mo^{4+}	Mo^{5+}	Mo^{6+}		image	sp^2C	sp^3C	$C_{oxidized}$
a	a1(229.1)	a2(230.4)	a3(232.5)		a’	a’1(284.5)	a’2(285.5)	a’3(288.5)
b	b1(229.5)	b2(231.1)	b3(232.5)		b’	b’1(284.4)	b’2(285.3)	b’3(288.3)
c	c1(229.0)	-	c2(232.5)		c’	c’1(284.3)	c’2(285.6)	c’3(286.3)

Figure 5. Mo 3d and C 1s XPS spectra.

Peaks in (a, b, c) assigned to carbidic Mo and peaks in (a′, b′, c′, d′) assigned to lattice C were marked with pentagram and cross, respectively. (a, a′) Eggshell $Mo_2C/\gamma\text{-}Al_2O_3$. (b, b′) Powder $Mo_2C/\gamma\text{-}Al_2O_3$. (c, c′) Powder Mo_2C. Assignation of the rest peaks was listed in the following table. As the peaks due to $d_{3/2}$ orbital (unmarked) were related with those due to $d_{5/2}$ orbital, here only listed the peaks due to the $d_{5/2}$ orbital of the Mo species in images a, b, c.

Table 3. PA Hydrogenation Performance Over Mo_2C Catalysts

Entry	WHSV (h^{-1})	Feed Rate (mL/min)	H_2/PA Molar Ratio	Powder Mo_2C Con.[a](%)	Powder Mo_2C Sel.[b](%)	Powder Mo_2C/γ-Al_2O_3 Con. (%)	Powder Mo_2C/γ-Al_2O_3 Sel. (%)	Eggshell Mo_2C/γ-Al_2O_3 Con. (%)	Eggshell Mo_2C/γ-Al_2O_3 Sel. (%)
1	2	0.03	204	97.3	91.2	99.7	0.1	99.2	91.2
2	4	0.06	204	95.9	92.4	98.3	70.9	98.3	93.4
3	6	0.09	204	91.7	92.7	98.0	84.7	96.9	94.1
4	8	0.12	204	78.8	94.3	97.9	84.5	96.4	94.6
5	10	0.15	204	72.7	94.4	98.0	88.2	95.8	95.4
6	12	0.18	204	63.2	94.5	96.1	89.4	95.2	95.7
7	16	0.24	204	47.0	94.7	95.0	90.3	95.2	95.9
8	20	0.30	204	41.5	94.7	94.7	91.2	91.6	96.1
9	20	0.30	102	–	–	–	–	92.4	96.8
10	20	0.30	20.4	–	–	–	–	94.3	97.4

[a]Conversion of PA.
[b]Selectivity to ST. Reaction temperature: 240°C. 2 MPa H_2.

about 20 h, it exhibited a catalytic performance resembling that of the eggshell Mo_2C/γ-Al_2O_3. We collected the Mo 3d XPS spectrum of the spent eggshell MoO_x/γ-Al_2O_3 and found a newly resolved peak assigned to carbidic Mo (Figure 7b), indicative of an exchange of the lattice oxygen in MoO_x with external carbon from reactants during the reaction, in which the process transformed the catalytic inert MoO_x into active MoC_x species.

Front-end PA hydrogenation

Conventionally, ST from EB dehydrogenation (Section I in Figure 8) first goes through heat exchange then condenses in the condenser to release H_2. The liquefied products are subject to Section II for manipulations (A: EB/ST separation column; B: EB recycle column; C: benzene/toluene separation column; D: ST rectifying column). The effluent of Section II is purified ST with untreated PA which shall be removed through PA hydrogenation process. Given that the molybdenum carbide catalysts for PA hydrogenation operated at high temperature (~240°C), we proposed putting the PA hydrogenation unit (Reactor A, Figure 8) between the heat exchanger and the condenser and use the tail-end cuts of Section I as the input for PA hydrogenation. The tail-end cuts are at high temperature (~550°C). The carried large amount of heat can be used to heat up the PA hydrogenation. By elevating the operating temperature of the PA hydrogenation to approach to that of the tail-end cuts, the energy loss of Route B can be significantly reduced. For Pd-based catalysts, the H_2/PA molar ratio had to be kept low, normally varying from 1 to 70, to suppress overhydrogenation. Hence, the existing PA hydrogenation processes can hardly be coupled with EB dehydrogenation process, where H_2 was far in excess of PA. To link up to the tail of EB dehydrogenation processes, the catalysts for PA hydrogenation should be designed to operate selectively in a wide range of H_2/PA ratios. The common value of H_2/PA in the tail-end cuts of EB dehydrogenation was around 100. Therefore, the H_2/PA ratio was first halved to 102. Both the ST selectivity and the PA conversion over the eggshell Mo_2C/γ-Al_2O_3 remained as high as 96.8 and 92.4%, respectively (Table 3, Entry 9), suggesting the catalyst could directly deal with the effluent of an EB dehydrogenation reactor in an effective manner. Even the H_2/PA ratio was reduced by 10 times, the conversion of PA remained high as 94.3% with the ST selectivity equal 97.3% (Table 3, Entry 10), indicating the eggshell Mo_2C/γ-Al_2O_3 was insensitive to the H_2/PA ratio that it was able to

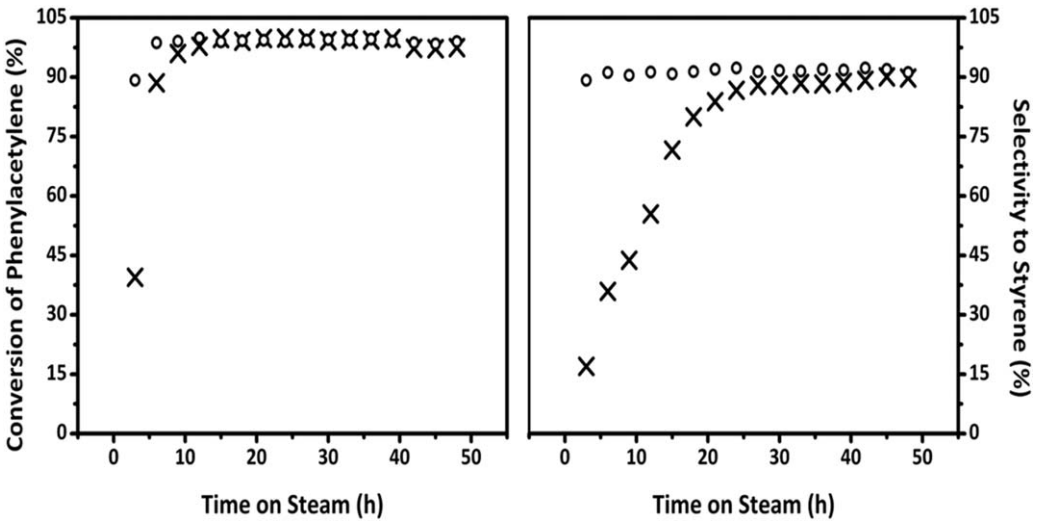

Figure 6. Time-dependency conversion of PA (a) and selectivity to ST (b) over the eggshell Mo_2C/γ-Al_2O_3 (o) and the eggshell MoO_x/γ-Al_2O_3 (x) in long-term PA hydrogenation.

Reaction conditions: 240°C, 2 MPa H_2, feed rate = 0.03 mL/min, H_2/PA = 204, WHSV = 2 h^{-1}.

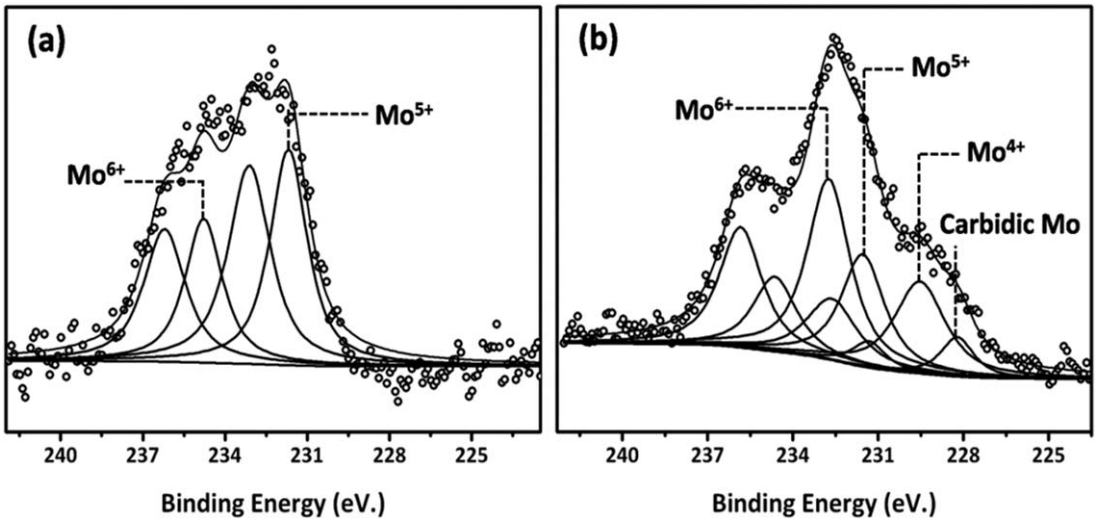

Figure 7. Mo 3d XPS spectra of the eggshell MoO_x/γ-Al_2O_3 before (a) and after (b) reaction.

Peak assignation: (a) Mo^{6+} species (236.2 eV, $3d_{3/2}$; 233.1 eV, $3d_{5/2}$), Mo^{5+} species (234.8 eV, $3d_{3/2}$; 231.7 eV, $3d_{5/2}$) and (b) Mo^{6+} species (235.8 eV, $3d_{3/2}$; 232.7 eV, $3d_{5/2}$), Mo^{5+} species (234.6 eV, $3d_{3/2}$; 231.5 eV, $3d_{5/2}$), Mo^{4+} species (232.6 eV, $3d_{3/2}$; 229.5 eV, $3d_{5/2}$), and carbidic Mo (231.3 eV, $3d_{3/2}$; 228.2 eV, $3d_{5/2}$).

conduct the PA hydrogenation effectively in a wide range of H_2/PA ratios.

Stability of eggshell Mo_2C/γ-Al_2O_3

To assess its feasibility for industrial application, we put the focus on the long-term performance of the eggshell Mo_2C/γ-Al_2O_3 in PA hydrogenation with excess ST in the feed. The catalyst exhibited a stable performance with steady activity and selectivity to ST in the 100 h life-time test (Figure 9a), showing potential for applications beyond lab scale. The effective elimination of PA was confirmed by the disappearance of the PA peak in gas chromatography, which was achieved after circulating the out-feed for three times (Figures 9b–d) with ST_{Loss} number of 4%.

PA hydrogenation under simulated industrial condition

One point that has to be recognized is the ability of the eggshell Mo_2C/γ-Al_2O_3 catalyst to eliminate the trace PA in a virtual sea of ST which was massively diluted by cyclohexane does not guarantee the usefulness of the catalyst in removing PA in a commercial ST plant, as the effluent from EB dehydrogenation reactor contains undiluted ST with a small amount of unreacted EB. Thus, to check whether the catalyst could be useful in commercial front-end PA hydrogenation, the catalyst was subjected to a mixture of ST and EB ($w:w = 90:10$) to find out if it could yet eliminate the involved trace PA. However, when the temperature was kept at 240°C, the ST flow suffered severe thermal polymerization in the reaction tube. Hopelessly, as the nonreaction zone of the reaction tube was about 16 times longer than the reaction zone, the long residence time of ST in the nonreaction zone does not permit a successful pass of concentrated ST through the reaction tube without thermal polymerization at temperature as high as 240°C. In this case, it was found only when the temperature was below 150°C could the thermal polymerization of the concentrated ST be alleviated to some

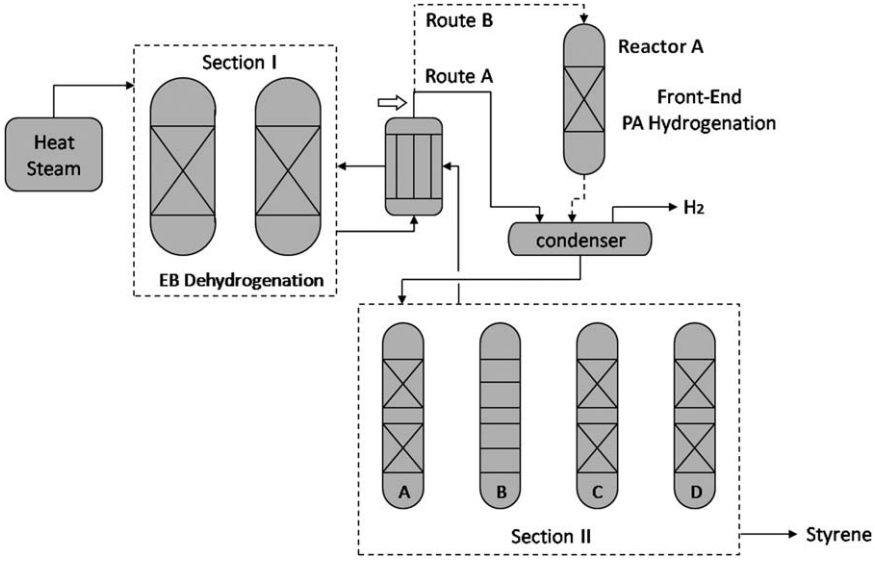

Figure 8. Illustration of the front-end PA hydrogenation technology.

Route A presented in solid line for production of ST via conventional route. Route B presented in dash line for production of ST monomers using front-end PA hydrogenation technique.

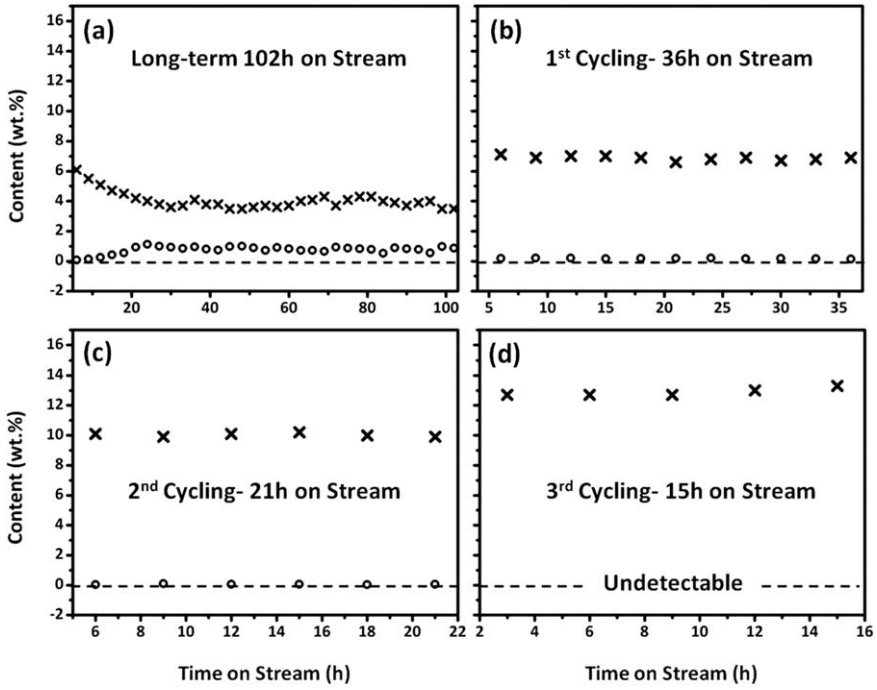

Figure 9. Time-dependency contents of PA (o) and EB (x) in the effluent of long-term PA-ST hydrogenation over the eggshell Mo_2C/γ-Al_2O_3.

The liquid products collected in the last hydrogenation process were used as the feedstock for the following hydrogenation process. Processes in a, b, c, and d were in time sequence. Reaction conditions: 240°C, 2 MPa H_2, H_2/PA molar ratio of 204, WHSV of 12 h^{-1}, initial feed: PA-ST (*w:w*, 10:90) diluted by 100 times in cyclohexane, feed rate of 0.18 mL/min. The content of each component was calculated on the basis of the total weight of PA + ST + EB. The catalyst was continuously on stream for 174 h in total.

extent within the specific type of reaction tube. In light of this, the reaction temperature was reduced to 120°C and the weight ratio of ST to EB was adjusted to near 50:50 to avoid the thermal polymerization of ST. In the meantime, the H_2 pressure was decreased to 0.3 MPa to lower the partial pressure of ST to avoid its hydrogenation, while the H_2 flow rate was set at 120 mL/min to accelerate the pass of ST through the reaction tube. In the first round, a mixture of EB and ST (*w:w* = 48:52) with 100 ppm PA relative to ST was introduced to the eggshell Mo_2C/γ-Al_2O_3 catalyst at liquid feed rate of 0.03 mL/min. The effluent from the hydrogenation reactor was found free of PA with EB:ST = 48:51 in weight. Then, the PA content in the EB-ST mixture was increased to 1000 ppm to check the response of the catalyst to bad situations in commercial production of ST. The results demonstrated the catalyst could respond well to the suddenly increased PA at bad working condition by eliminating PA without losing ST. These preliminary results proved that the eggshell Mo_2C/γ-Al_2O_3 catalyst by virtue of molybdenum carbide being ineffective in activating ST suits for the PA removal within excess ST at high concentration. Therefore, it might develop into a cost-effective catalyst for commercial front-end purification of ST monomers. One thing we have to acknowledge is, in this case reducing the reaction temperature to 120°C is against the proposed energy integration concept, which may also undermine the eggshell Mo_2C/γ-Al_2O_3 catalyst's advantage of being able to steadily work at high temperature in contrast to the Pd-based catalysts. But it is believed that, through reducing the aspect ratio of the hydrogenation reactor and decreasing the portion of the non-reaction zone to a certain degree, the thermal polymerization problem of ST can be mitigated. Accordingly, the reaction temperature needs further optimization. Furthermore, given the industrial use of steam diluent as a heat source in EB dehydrogenation reactor, the effect of steam on the performance of the eggshell Mo_2C/γ-Al_2O_3 catalyst should be investigated on the potential use of the catalyst in PA removal in a commercial ST plant.

Conclusions

In summary, localizing Mo_2C in a nanosized eggshell proved to be a unique way to utilize the intrinsic selective character of Mo_2C in PA hydrogenation while maintaining a high PA turnover rate. The eggshell Mo_2C/γ-Al_2O_3 catalysts with a significantly lower cost than noble metal catalysts can operate effectively with a wide concentration window for gas-phase PA hydrogenation. The preliminary results indicate the carbide catalyst might potentially be used for economical coupled processes for the front-end purification of alkenes in chemical industry.

Acknowledgments

The authors acknowledge the financial support provided by the National Natural Science Foundation of China (21373038 and 21428301). The authors thank Mr. Guangyi Li for measuring the TPO profiles of the catalysts, and Dr. Alex C. W. Tsang for the improvement in English.

Literature Cited

1. Domínguez-Domínguez S, Berenguer-Murcia Á, Cazorla-Amorós D, Linares-Solano Á. Semihydrogenation of phenylacetylene catalyzed by metallic nanoparticles containing noble metals. *J Catal*. 2006; 243:74–81.
2. Starodubtseva EV, Vinogradov MG, Turova OV, Bumagin NA, Rakov EG, Sokolov VI. Palladium(0) supported on carbon nanotubes

as an efficient catalyst of the C≡C bond hydrogenation. *Catal Commun*. 2009;10:1441–1442.
3. Shao ZF, Li C, Chen X, Pang M, Wang XK, Liang CH. A facile and controlled route to prepare an eggshell Pd catalyst for selective hydrogenation of phenylacetylene. *ChemCatChem*. 2010;2:1555–1558.
4. Domínguez-Domínguez S, Berenguer-Murcia Á, Linares-Solano Á, Cazorla-Amorós D. Inorganic materials as supports for palladium nanoparticles: application in the semi-hydrogenation of phenylacetylene. *J Catal*. 2008;257:87–95.
5. Weerachawanasak P, Mekasuwandumrong O, Arai M, Fujita S-I, Praserthdam P, Panpranot J. Effect of strong metal–support interaction on the catalytic performance of Pd/TiO_2 in the liquid-phase semihydrogenation of phenylacetylene. *J Catal*. 2009;262:199–205.
6. Liu W, Arean CO, Bordiga S, Groppo E, Zecchina A. Selective phenylacetylene hydrogenation on a polymer-supported palladium catalyst monitored by FTIR spectroscopy. *ChemCatChem*. 2011;3:222–226.
7. Deng DS, Yang Y, Gong YT, Li Y, Xu X, Wang Y. Palladium nanoparticles supported on mpg-C_3N_4 as active catalyst for semihydrogenation of phenylacetylene under mild conditions. *Green Chem*. 2013;15:2525–2531.
8. Crespo-Quesada M, Cárdenas-Lizana F, Dessimoz A-L, Kiwi-Minsker L. Modern trends in catalyst and process design for alkyne hydrogenations. *ACS Catal*. 2012;2:1773–1786.
9. Zhang QW, Li J, Liu XX, Zhu QM. Synergetic effect of Pd and Ag dispersed on Al_2O_3 in the selective hydrogenation of acetylene. *Appl Catal A*. 2000;197:221–228.
10. Osswald J, Kovnir K, Armbrüster M, Giedigkeit R, Jentoft RE, Wild U, Grin Y, Schlögl R. Palladium–gallium intermetallic compounds for the selective hydrogenation of acetylene: part II: surface characterization and catalytic performance. *J Catal*. 2008;258:219–227.
11. Guczi L, Schay Z, Stefler G, Liotta LF, Deganello G, Venezia AM. Pumice-supported Cu–Pd catalysts: influence of copper on the activity and selectivity of palladium in the hydrogenation of phenylacetylene and but-1-ene. *J Catal*. 1999;182:456–462.
12. Crespo-Quesada M, Yarulin A, Jin MS, Xia YN, Kiwi-Minsker L. Structure sensitivity of alkynol hydrogenation on shape- and size-controlled palladium nanocrystals: which sites are most active and selective? *J Am Chem Soc*. 2011;133:12787–12794.
13. Tao AR, Habas S, Yang PD. Shape control of colloidal metal nanocrystals. *Small*. 2008;4:310–325.
14. Weerachawanasak P, Mekasuwandumrong O, Arai M, Fujita SI, Praserthdam P, Panpranot J. Effect of strong metal–support interaction on the catalytic performance of Pd/TiO_2 in the liquid-phase semihydrogenation of phenylacetylene. *J Catal*. 2009;262:199–205.
15. Lee KH, Lee B, Lee KR, Yi MH, Hur NH. Dual Pd and $CuFe_2O_4$ nanoparticles encapsulated in a core/shell silica microsphere for selective hydrogenation of arylacetylenes. *Chem Commun*. 2012;48:4414–4416.
16. Tschan R, Wandeler R, Schneider MS, Schubert MM, Baiker A. Continuous semihydrogenation of phenylacetylene over amorphous $Pd_{81}Si_{19}$ alloy in "supercritical" carbon dioxide: relation between catalytic performance and phase behavior. *J Catal*. 2001;204:219–229.
17. Crespo-Quesada M, Andanson JM, Yarulin A, Lim B, Xia YN, Kiwi-Minsker L. UV–ozone cleaning of supported poly(vinylpyrrolidone)-stabilized palladium nanocubes: effect of stabilizer removal on morphology and catalytic behavior. *Langmuir*. 2011;27:7909–7916.
18. Evangelisti C, Panziera N, D'Alessio A, Bertinetti L, Botavina M, Vitulli G. New monodispersed palladium nanoparticles stabilized by poly-(N-vinyl-2-pyrrolidone): preparation, structural study and catalytic properties. *J Catal*. 2010;272:246–252.
19. Nikolaev SA, Smirnov VV. Selective hydrogenation of phenylacetylene on gold nanoparticles. *Gold Bull*. 2009;42:182–189.
20. Nikolaev SA, Smirnov VV. Synergistic and size effects in selective hydrogenation of alkynes on gold nanocomposites. *Catal Today*. 2009;147:336–341.
21. Studt F, Abild-Pedersen F, Bligaard T, Sørensen RZ, Christensen CH, Nørskov JK. Identification of non-precious metal alloy catalysts for selective hydrogenation of acetylene. *Science*. 2008;320:1320.
22. Lee KH, Lee B, Lee KR, Yi MH, Hur NH. Dual Pd and $CuFe_2O_4$ nanoparticles encapsulated in a core/shell silica microsphere for selective hydrogenation of arylacetylenes. *Chem Commun*. 2012;48:4414–4416.
23. Bridier B, Pérez-Ramírez J. Cooperative effects in ternary Cu−Ni−Fe catalysts lead to enhanced alkene selectivity in alkyne hydrogenation. *J Am Chem Soc*. 2010;132:4321–4327.
24. Nitta Y, Matsugi S, Imanaka T. Partial hydrogenation of phenylacetylene on copper-promoted iron catalyst. *Catal Lett*. 1990;5:67–72.
25. Tew MW, Janousch M, Huthwelker T, Bokhoven JA. The roles of carbide and hydride in oxide-supported palladium nanoparticles for alkyne hydrogenation. *J Catal*. 2011;283:45–54.
26. Pang M, Wang XK, Xia W, Muhler M, Liang CH. Mo(VI)–Melamine hybrid as single-source precursor to pure-phase β-Mo_2C for the selective hydrogenation of naphthalene to tetralin. *Ind Eng Chem Res*. 2013;52:4564–4571.
27. Gibson EK, Zandbergen MW, Jacques SDM, Biao C, Cernik RJ, O'Brien MG, Michiel MD, Weckhuysen BM, Beale AM. Noninvasive spatiotemporal profiling of the processes of impregnation and drying within Mo/Al_2O_3 catalyst bodies by a combination of X-ray absorption tomography and diagonal offset Raman spectroscopy. *ACS Catal*. 2013;3:339–347.
28. Wolden CA, Pickerell A, Gawai T, Parks S, Hensley J, Way JD. Synthesis of β-Mo_2C thin films. *ACS Appl Mater Interfaces*. 2011;3:517−521.
29. Pang M, Liu CY, Xia W, Muhler M, Liang CH. Activated carbon supported molybdenum carbides as cheap and highly efficient catalyst in the selective hydrogenation of naphthalene to tetralin. *Green Chem*. 2012;14:1271–1276.
30. Levy RB, Boudart M. Platinum-like behavior of tungsten carbide in surface catalysis. *Science*. 1973;181:547–548.
31. Chen JG. Carbide and nitride overlayers on early transition metal surfaces: preparation, characterization, and reactivities. *Chem Rev*. 1996;96:1477–1498.
32. Hwu HH, Chen JG. Surface chemistry of transition metal carbides. *Chem Rev*. 2005;105:185–212.
33. Nelmark AV, Kheifez LI, Fenelonov VB. Theory of preparation of supported catalysts. *Ind Eng Chem Prod Res Dev*. 1981;20:439–450.
34. Dougherty RC, Verykios XE. Nonuniformly activated catalysts. *Catal Rev Sci Eng*. 1987;29:101–150.

Manuscript received May 14, 2014, and revision received Mar. 27, 2015.